DECOMPOSITION OF SUPERCOOLED AUSTENITE IN CONTINUOUS COOLING TRANSFORMATION PROCESS OF A Mn-Mo-Ni LOW ALLOY STEEL

C. W. Li, L. Z. Han, Q. D. Liu, X. G Tao, J. F. Gu, W. M. Zhang

Institute of Materials Modification and Modeling, School of Materials Science and Engineering, Shanghai Jiao Tong University; 800 Dong Chuan Road; Shanghai, 200240, PR China

Keywords: Mn-Mo-Ni low alloy steel, Austenite decomposition, hardness

Abstract

Decomposition of supercooled austenite in continuous cooling transformation process of a Mn-Mo-Ni low alloy steel was evaluated by dilatometric measurements, light microscopy, electron backscatter diffraction, and microhardness testing and other methods. The results show that at the cooling rates of 1°C/s or below, ferrite initially formed and continuously rejecting C into the untransformed austenite, which transforms to C-rich lower bainite at lower temperature, resulting in ferrite-bainite dual-phase microstructures. At the cooling rates between 1 °C/s and 5 °C/s, the successive transformation products are bainite ferrite, upper bainite and lower bainite, and islands of carbon-enriched austenite transform to martensite (plus retained austenite) at low temperatures. The upper bainite and martensite dual-phase microstructures are formed at the range of 5 °C/s to 50 °C/s with a lower M_s. When cooling rates greater than approximately 50 °C/s, the microstructure are martensite and retained austenite at room temperature. With the increase of cooling speed, the residual austenite content increased before decreased at the cooling speed of 2 °C/s, which is probably associated with the incompleteness of bainite transformation.

Introduction

The safety and longevity of nuclear power plants is very important for human society[1, 2]. The structural integrity of the reactor pressure vessel is vital for the safety of the entire nuclear power plant and determines the ultimate service life-span [3-5]. The Mn-Mo-Ni low alloy steels are key materials used for the fabrication of nuclear reactor facilities, such as reactor pressure vessels, steam generators, and compressors[6, 7]. In the past 40 years, the neutron irradiation embrittlement[8], ductile-brittle transition temperature[9], fracture toughness[10, 11] and other properties[12] of Mn-Mo-Ni low alloy steels have been extensively studied, and the results certified that they show an excellent combination of irradiation resistance and other properties required for the application in third generation nuclear power reactors.

In order to prolong the third generation's life-span to more than 60 years, the pressure vessels are bigger and heavier than before, and the integrated design was used to reduce the welding[13]. That is to say, the steel needs to do in-depth research to discover the potential properties. Then, the appropriate processing should be adopted to enhance the performance of the big forging, and then, assure the reliability of nuclear power security.

The heat treatment is the last procedure of thermal manufacturing of large forgings before delivery, it decides the microstructure, and has direct influence with the performance of the large forgings[14]. However, the current heat treatment technology is difficult to guarantee these

forgings production because these heave forgings reach to 500 tons due to abnormity and the large volume，and there is not much research on the heat treatment of these forgings steels because people paid more attention to metallurgy, foundry, and forging technology. With the improvement of big ingot casting and forging forming and the further quality requirements, people realize that heat treatment has a big influence to the microstructure and mechanical properties of big forging, particularly, the quenching cooling speed[15].

The different parts of a forging have different quenching cooling rate because of it's the large volume; this must result in the differences in the performance. Although the continuous cooling transformation (CCT) diagram[16] has been determined and the qualitative relationship between the cooling speed and microstructure has been identified in previous studies, a quantitative dependence of cooling rate on the mechanical properties is not perfected yet.

Materials and Experiments

The chemical composition of the Mn-Mo-Ni low alloy steel investigated is listed in Table 1, and the samples after preliminary heat treatment have a mixture microstructure of ferrite (54 vol. %) and bainite (46 vol. %) with the grain size was approx. 25 μm.

Table 1 chemical composition of the investigated steel (wt.%).

Steel	C	Mn	Ni	Mo	Cr	Si	Cu	Al	Fe
	0.17	1.41	0.82	0.51	0.13	0.17	0.03	0.011	Bal.

The simulated experiments were carried out with a DIL 805A machine. Specimens, 10 mm in length and 4 mm in diameter, were prepared for the thermal simulation experiments. he simulated specimens were heated to 900 °C in 3 min, held at this temperature for 30 min and then cooled to room temperature at a rate varying from 100 °C/s to 0.02 °C/s. In the process of simulation tests, the machine could record the changes of thermal expansion rates with temperature and time automatically. The expansion curves recording the phase transformation temperature and expansion rates could be achieved. The austenitizing start temperature (A_{c1}), the austenitizing finish temperature (A_{c3}) and the martensite start temperature (M_s), etc. were determined using the tangent curve method.

Optical microscopy (OM) and electron backscatter diffraction (EBSD) were used to observe the microstructure of the specimens after after simulation tests. The OM specimens were mechanically polished before etched with a 4% Nital solution. The EBSD specimens were polished via 50 nm colloidal silica after mechanically polished to 0.5 μm surface roughness. Then, they observed under an optical microscope (Zeiss Axiovert 200 MAT) and an FEI field-emission scanning electron microscope (NOVA NanoSEM 230) equipped with a HKL-EBSD fast acquisition system, respectively. The hardness tests were conducted using a HR-150A Vickers sclerometer, with a load of 980N (10kg) and a holding time of 15s.

Results and discussions

Microstructure

The microstructure observations of the Mn-Mo-Ni low alloy steel with different cooling rates are shown in Fig. 1. When the cooling rates were 0.05 °C/s and 0.2 °C/s, 72% and 44% ferrite

microstructure were obtained (Fig. 1a-b), respectively. When the cooling rates increased to 1 °C/s and 2°C/s, there was no ferrite transformation region on the dilatometric curve (shown in Fig. 2b), but a small amount of ferrite formed as shown in Fig. 1c. Therefore, the cooling rate of 1 °C/s could be considered as the critical cooling rate to achieve the ferrite microstructure. When the cooling rates were 5 °C/s and 10 °C/s, almost complete, 79% and 35% bainite microstructure were obtained (Fig. 1d-e), respectively. When the cooling rates decreased to 50 °C/s, there was no bainite transformation region on the dilatometric curve (shown in Fig. 2b), but a small amount of bainitic ferrite formed as shown in Fig. 1f. Therefore, the cooling rate of 50 °C/s could be considered as the critical cooling rate to achieve the bainite microstructure. The cooling rates, which higher than 50 °C/s, corresponded to fully martensite transformations, as shown in Fig. 2b. The martensite grains took on a typical lath like appearance and the cooling rates had little influence on the martensite morphology. There was no martensite transformation region on the dilatometric curve when the cooling rate lower than 2 °C/s as shown in Fig. 2, but some martensite islands could be observed in the OM. The carbon content of martensite islands were higher than the martensite obtained at high cooling rate due to the carbon contributed to undecomposed austenite.

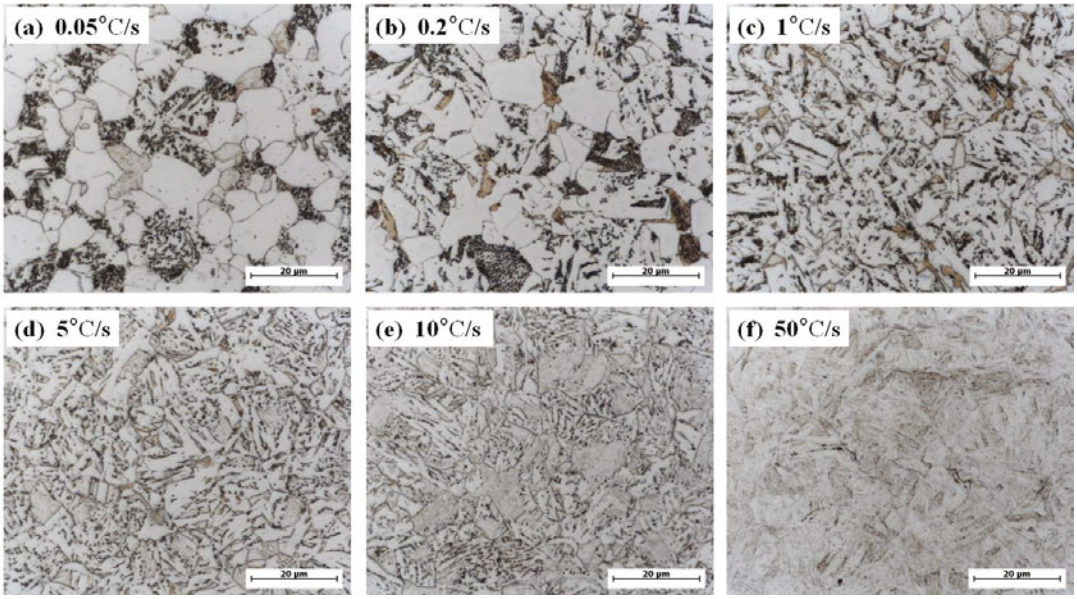

Figure 1 Microstructure of specimens cooled at various cooling rates, light micrographs. F_B: bainitic ferrite; M-A: martensite-austenite island.

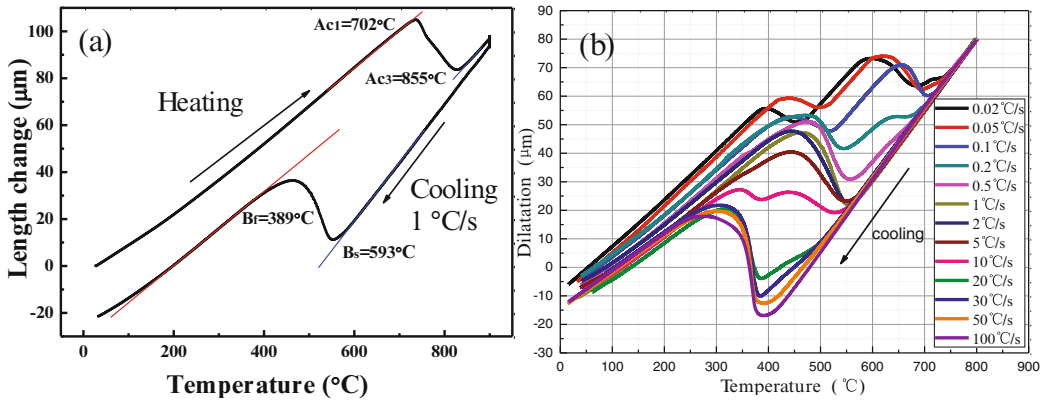

Figure 2 Dilatation curves obtained for various cooling rates.

Figure 3 compares the combination of image quality maps and phase distribution images of the steel with different cooling rate obtained by EBSD. Red areas denote retained austenite, while the others consist of a *bcc* phase including martensite marked in black, bainite marked in gray and ferrite marked in white. It was found that matensite were found in full cooling rate range, and the austenites were found in the cluster of bainite. Figure 4 shows the retained austenite content of the steel with different cooling rate. It is demoted that with decreased cooling rate, the retained austenite content, which is tested by XRD, initially increases from 0.5% to 10%, and then decreases to 1%, with a maximum value at 2 °C/s which probably associated with the incompleteness of bainite transformation.

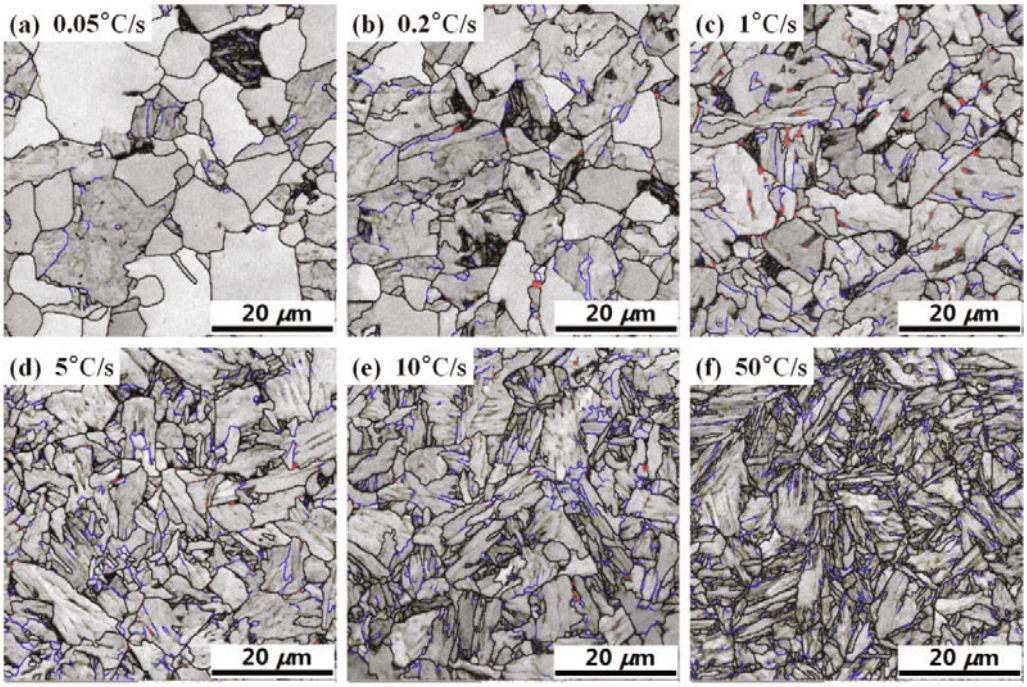

Figure 3 The micrographs showing phase distribution, based on EBSD image quality maps, of the steel cooled at different rates (a) 0.05 °C/s, (b) 0.2 °C/s, (c) 1 °C/s, (d) 5 °C/s, (e) 10 °C/s, (f) 50 °C/s, F_B: bainitic ferrite; A: austenite areas in red; M: martensite areas in black.

Dilatometric curves

The dilatometric curves of different cooling rates were obtained using a DIL 805A machine. On the dilatometric curves (Fig .2), the average temperatures of A_{c1}, A_{c3}, M_s and M_f were 702 °C, 855 °C, 428 °C and 260 °C, respectively, determined by the tangent method. The starting and finishing temperatures of the bainite transformation were achieved using the same method and were 583 °C and 389 °C respectively at 1 °C/s. The starting and finishing temperatures of the ferrite transformation were 537 °C and 614 °C respectively, using the 0.1 °C/s cooling rate data, and at the same cooling rate, the bainite transformation starting and finishing temperatures were 537 °C and 341 °C which is lower than the starting and finishing temperatures at 1 °C/s. The reason of this phenomenon is the carbon content of bainite were higher than the average content of austenite due to the carbon contributed to undecomposed austenite.

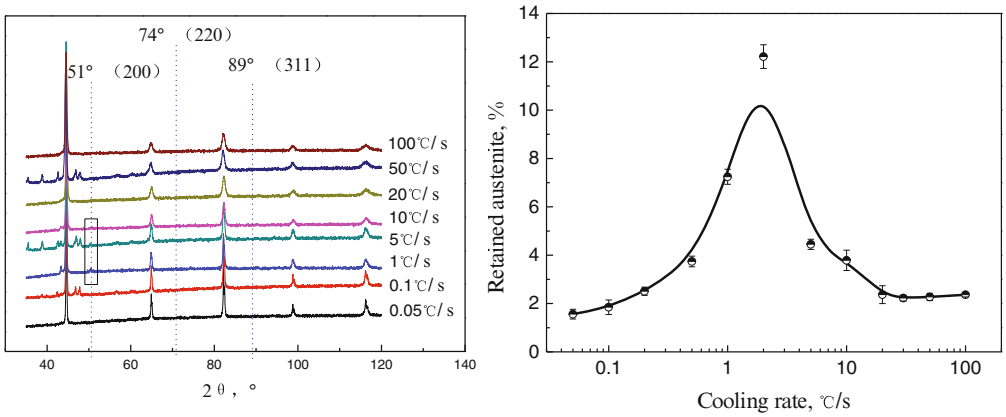

Figure 4 Retained austenite content at room temperature of specimens with different cooling rates, the austenite distribution photos are shown in the diagram.

Microhardness

Figure 5 shows the measured average Vickers hardness values of the investigated samples cooled down to room temperature at different rates in the range of 100-0.05 °C/s. It was found that the measured Vickers hardness values of the experimental steel do not increase linearly with the increasing applied cooling rate. In detail, the curve in Fig. 5 can be divided into four separated stages (as indicated in the figure): (I) hardness increasing rapidly with the cooling rate of 0.05–0.2 °C/s; (II) reaching a plateau stage between 0.2 and 2 °C/s; (III) hardness increasing rapidly with the cooling rate from 2 °C/s to 30 °C/s; (IV) when the cooling rates were higher than 30 °C/s, the microhardness values were 398–405 HV, and this indicated that the cooling rate had little influence on the microhardness.

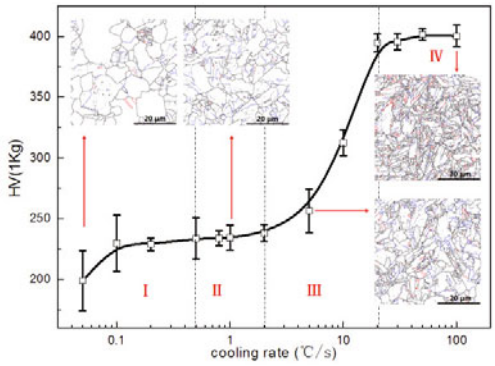

Figure 5 Measured Vickers hardness values of specimens cooled down to room temperature from the austenite region at various rates in the range of 0.05 °C/s - 100 °C/s

The big angle grain boundary distribution of 0.05 °C/s, 1 °C/s, 10 °C/s, 100 °C/s were shown in the Fig.5, responded of ferrite and bainite, bainite, bainite and martensite, martensite respectively. It is can be found that the big grain boundary length increased with the cooling rate. The increase in hardness observed in this cooling range can be associated with the reduction in the effective grain size, as quantified in the figure, and is probably also associated with the contribution of some precipitation and Solid solubility of matrix.

Conclusions

Influence of cooling rates on the microstructures of Mn-Mo-Ni low alloy steel was studied. The following conclusions were obtained: at the cooling rates of 1 °C/s or below, ferrite initially formed and continuously rejecting C into the untransformed austenite, which transforms to C-rich lower bainite at lower temperature, resulting in ferrite-bainite dual-phase microstructures. At the cooling rates between 1 °C/s and 10 °C/s, the successive transformation products are bainite ferrite, upper bainite and lower bainite. The upper bainite and martensite dual-phase microstructures are formed at the range of 10 °C/s to 50 °C/s with a lower M_s. When the cooling rates ranged from 100 °C/s to 50 °C/s, fully martensitic transformations were achieved and the cooling rate had very little influence on the microstructure of the martensite. With the increase of cooling speed, the residual austenite content increased before decreased at the cooling speed of 2 °C/s, which is probably associated with the incompleteness of bainite transformation.

Acknowledgements

This work was financially supported by the National Basic Research Program of China under Grant No. 2011CB012904, and China Postdoctoral Science Foundation under Grant No. 2013M541517.

References

1. Zinkle, S.J. and G.S. Was, Materials challenges in nuclear energy. Acta Materialia, 2013. 61(3): p. 735-758.
2. Yvon, P. and F. Carré, Structural materials challenges for advanced reactor systems. Journal of Nuclear Materials, 2009. 385(2): p. 217-222.
3. Pous-Romero, H. and H.K. Bhadeshia, Continuous Cooling Transformations in Nuclear Pressure Vessel Steels. Metallurgical and Materials Transactions A, 2014. 45(11): p. 4897-4906.
4. Pous-Romero, H., et al., Austenite grain growth in a nuclear pressure vessel steel. Materials Science and Engineering: A, 2013. 567(0): p. 72-79.
5. Takayama, N., G. Miyamoto, and T. Furuhara, Effects of transformation temperature on variant pairing of bainitic ferrite in low carbon steel. Acta Materialia, 2012. 60(5): p. 2387-2396.
6. Lee, K.-H., et al., Evaluation of microstructural parameters controlling cleavage fracture toughness in Mn–Mo–Ni low alloy steels. Materials Science and Engineering: A, 2013. 565: p. 158-164.
7. Kempf, R., H. Troiani, and A.M. Fortis, Effect of lead factors on the embrittlement of RPV SA-508 cl 3 steel. Journal of Nuclear Materials, 2013. 434(1-3): p. 411-416.
8. Kim, M.-C., et al., Comparison of fracture properties in SA508 Gr. 3 and Gr. 4N high strength low alloy steels for advanced pressure vessel materials. International Journal of Pressure Vessels and Piping, 2015.
9. Ma, N., L. Wang, and Y. Chen, A508-3 Steel Ductile-Brittle Transition Temperature Range Fracture Toughness Research. Nucl. Power Eng, 2012. 33(2): p. 56-60.
10. Erickson, M., et al. The Role of Grain Size in Predicting Cleavage Fracture Toughness of Pressure Vessel Steels. in ASME 2013 Pressure Vessels and Piping Conference. 2013.

American Society of Mechanical Engineers.
11. Gopalan, A., M. Samal, and J. Chakravartty, Fracture toughness evaluation of 20MnMoNi55 pressure vessel steel in the ductile to brittle transition regime: Experiment & Numerical simulations. Journal of Nuclear Materials, 2015.
12. Robertson, C.F., K. Obrtlik, and B. Marini, Dislocation structures in 16MND5 pressure vessel steel strained in uniaxial tension at different temperatures from −196°C up to 25°C. Journal of Nuclear Materials, 2007. 366(1-2): p. 58-69.
13. Koundy, V., et al., Study of tearing behaviour of a PWR reactor pressure vessel lower head under severe accident loadings. Nuclear Engineering and Design, 2008. 238(9): p. 2411-2419.
14. G. R. Wei, D.C.F., S. Z. Huang, et.al., The study of heat treatment of A508-3 steel. nuclear Power Engineering, 1989. 10(3): p. 266-270.
15. Z.Q. Sheng, H.X., F. peng, The microstructures os A508-3 steel after heat treatment. Nuclear Power Engineering, 1988. 9(1): p. 49-53.
16. Niffenegger, M. and H.J. Leber, Monitoring the embrittlement of reactor pressure vessel steels by using the Seebeck coefficient. Journal of Nuclear Materials, 2009. 389(1): p. 62-67.